J Arid Land (2025) 17(11): 1558–1575
doi: 10.1007/s40333-025-0065-z; CSTR: 32276.14.JAL.0250065z

Science Press Springer-Verlag

Spatial variability characteristics and drivers of surface soil nitrogen fractions in the drylands of northern China

ZHANG Shihang[1,2], CHEN Yusen[2,3], ZHOU Xiaobing[3*], ZHANG Yuanming[3]

[1] Key Laboratory of Mountain Surface Processes and Ecological Regulation, Institute of Mountain Hazards and Environment, Chinese Academy of Sciences, Chengdu 610041, China;
[2] University of Chinese Academy of Sciences, Beijing 100049, China;
[3] State Key Laboratory of Ecological Safety and Sustainable Development in Arid Lands, Xinjiang Institute of Ecology and Geography, Chinese Academy of Sciences, Urumqi 830011, China

Abstract: In dryland ecosystems, nitrogen (N) is the primary limiting factor after water availability, constraining both plant productivity and organic matter decomposition while also regulating ecosystem function and service provision. However, the distributions of different soil N fraction stocks in drylands and the factors that influence them remain poorly understood. In this study, we collected 2076 soil samples from 173 sites across the drylands of northern China during the summers of 2021 and 2022. Using the best-performing eXtreme Gradient Boosting (XGBoost) model, we mapped the spatial distributions of the soil N fraction stocks and identified the key drivers of their variability. Our findings revealed that the stocks of total nitrogen (TN), inorganic nitrogen (IN), and microbial biomass nitrogen (MBN) in the top 30 cm soil layer were 1020.4, 92.2, and 40.8 Tg, respectively, with corresponding mean densities of 164.6, 14.9, and 6.6 g/m^2. Climate variables—particularly mean annual temperature and aridity—along with human impacts emerged as the dominant drivers of soil N stock distribution. Notably, increased aridity and intensified human impacts exerted mutually counteracting effects on soil N fractions: aridity-driven moisture limitation generally suppressed N accumulation, whereas anthropogenic activities (e.g., fertilization and grazing) promoted N enrichment. By identifying the key environmental and anthropogenic factors shaping the soil N distribution, this study improves the accuracy of regional and global N stock estimates. These insights provide a scientific foundation for developing more effective soil N management strategies in dryland ecosystems, contributing to sustainable land use and long-term ecosystem resilience in drylands.

Keywords: soil nitrogen fractions; total nitrogen (TN); inorganic nitrogen (IN); microbial biomass nitrogen (MBN); machine learning model; eXtreme Gradient Boosting (XGBoost) model; dryland ecosystems

Citation: ZHANG Shihang, CHEN Yusen, ZHOU Xiaobing, ZHANG Yuanming. 2025. Spatial variability characteristics and drivers of surface soil nitrogen fractions in the drylands of northern China. Journal of Arid Land, 17(11): 1558–1575. https://doi.org/10.1007/s40333-025-0065-z; https://cstr.cn/32276.14.JAL.0250065z

1 Introduction

Drylands, characterized by an aridity index (AI)—the ratio of mean annual precipitation to mean annual potential evapotranspiration—of less than 0.65, represent the Earth's largest terrestrial

*Corresponding author: ZHOU Xiaobing (E-mail: zhouxb@ms.xjb.ac.cn)
The first and second authors contributed equally to this work.
Received 2025-03-09; revised 2025-06-10; accepted 2025-06-14

biome, covering about 45.0% of the planet's surface and supporting over 2.5×10^9 people (Schimel, 2010). These regions provide vital ecosystem services, including food, fiber, biofuel, and biodiversity, to rapidly growing populations worldwide (Reynolds et al., 2007). Arid ecosystems are highly susceptible to external environmental changes (Wang et al., 2014), making research on these ecosystems essential for the survival and development of humanity in the future.

By 2025, drylands are projected to occupy 48.0% of the global land area and account for 51.0% of the global population growth between 2000 and 2025, with 50.0% of this growth occurring in developing countries and only 1.0% in developed countries (Huang et al., 2016). China, the largest developing country in the world, has a dryland region of about 6.6×10^6 km^2, home to 5.8×10^8 people (Li et al., 2021). However, dryland ecosystems in China are extremely fragile and have low stability (Maestre et al., 2015; Li et al., 2021), making them one of the most sensitive areas to climate change and human activities. China's drylands are located primarily in the northern region. Therefore, under global change, strengthening research on soil properties in the drylands of northern China is crucial for enhancing the resilience of global dryland ecosystems and building cross-regional ecological barriers.

Nitrogen (N) is a fundamental growth-limiting nutrient for plants (Liu et al., 2017a) and an essential element for all life forms on the Earth (Galloway et al., 2004). In drylands, N is the primary factor limiting ecosystem net primary productivity and organic matter decomposition (Hu et al., 2017). Consequently, N cycling is central to ecosystem functioning and service provisioning in these regions (Compton et al., 2011; Elrys et al., 2024). Soil is the principal reservoir of N in terrestrial ecosystems and contains more N than vegetation does (Pinder et al., 2013). Xu et al. (2020) assessed terrestrial ecological N stocks in China and reported that the total nitrogen (TN) stock in the 0–100 cm soil layer was 10.14 Pg—about 35 times greater than that in vegetation (0.29 Pg). The dynamics of soil N determine whether a terrestrial ecosystem functions as a N sink or source (Tian et al., 2006) and can even influence the biogeochemical cycles of other ecosystems (Luo et al., 2004). According to Plaza et al. (2018), soil N is primarily concentrated in the topsoil (0–30 cm). While TN indicates the size of the soil N pool, it does not fully capture the quality or variability of that pool (Pu et al., 2019). Previous research has focused largely on estimating TN stocks in individual forests or grasslands (He et al., 2008; Liu et al., 2013; Kou et al., 2019; Zhang et al., 2020).

Soil microbes, as the primary decomposers in terrestrial ecosystems, play critical roles in driving and regulating ecological processes (Bardgett and van der Putten, 2014). They contribute to essential nutrient cycling functions, including soil carbon sequestration (Spohn, 2016), organic matter decomposition (Heuck et al., 2015), N mineralization, nutrient cycling (Handa et al., 2014), and soil formation (Rillig and Mummey, 2006). Among these processes, soil microbial biomass nitrogen (MBN) acts as a central intermediary in the transformation of organic nitrogen (ON) to inorganic nitrogen (IN), playing a key role in the carbon and N cycles of ecosystems (Powlson et al., 1987). MBN also serves as a critical biological indicator for assessing soil quality and health, and it is an important source of available nutrients closely associated with plant root nutrition (Gao et al., 2022).

Soil N distribution is highly spatially heterogeneous (Liu et al., 2013) and influenced by various factors, including climate change (Kou et al., 2019), land use/land cover (LULC) (Meena et al., 2018), human impacts (Delgado-Baquerizo et al., 2016), soil physical and chemical properties (Durán et al., 2018), and vegetation. Climate change primarily affects soil N through alterations in environmental factors such as temperature and precipitation. For example, global warming—resulting in warmer and wetter climates—enhances soil N mineralization (Liu et al., 2017b), thereby impacting soil TN stocks. In drylands, reduced precipitation can adversely affect microbial growth and nutrient dispersal in the soil (Davidson and Janssens, 2006; Sardans et al., 2008), leading to decreased microbial metabolic activity and influencing TN stocks. Changes in LULC can lead to shifts in soil organic carbon and TN stocks (Gross and Harrison, 2019). Numerous studies have demonstrated a strong relationship between the soil nutrient status in the

surface layer and LULC type, with natural ecosystems (including forests, shrublands, and grasslands) exhibiting higher soil nutrient levels than croplands (Elrys et al., 2023; Yang et al., 2023; Zhu et al., 2025). Soil accumulation under nutrient patterns varies with vegetation succession (Zhang et al., 2013; Zhang et al., 2015; Liu et al., 2017a).

Human impacts, including grazing, fertilization, intensive agriculture, and fossil fuel combustion, alter both N inputs and losses in global terrestrial ecosystems (Cui et al., 2013). For example, Fujimaki et al. (2009) reviewed the ecological risks associated with N saturation in natural terrestrial ecosystems due to anthropogenic disturbances. Wang et al. (2019) identified human impacts as significant drivers of changes in the N cycle in northern China. In recent years, global anthropogenic N inputs have doubled the amount of naturally fixed TN in terrestrial and aquatic ecosystems, resulting in annual depositions of ON and IN of about 124 Tg/a (Cornell, 2011). The current global average N deposition rate already exceeds 10.00 kg/(hm^2·a) in most regions (Dentener et al., 2006), and the annual average soluble N deposition in atmospheric wet deposition in China reaches 13.69 kg/hm^2 (Zhu et al., 2016).

Among soil physical and chemical properties, factors such as pH and soil sand content have been found to be correlated with the spatial variability of N (Durán et al., 2018). Understanding the combined direct and indirect effects of climate change, human impacts, vegetation changes, and soil physical and chemical properties on alterations in N fractions is critical for improving predictions of the ecological consequences of ongoing global change in terrestrial ecosystems (Delgado-Baquerizo et al., 2016). N absorbed by plants is primarily inorganic, mainly in the form of NH_4^+-N and NO_3^--N, whereas ON (such as amino acids and nucleic acids) is absorbed in much smaller quantities (Zhan, 2022). More than 90.0% of the soil N exists in organic form, whereas only 2.0%–8.0% is present in inorganic form. Numerous studies have shown that the soil IN content in arid ecosystems is influenced by factors such as climate, shrub species, spatial location, and soil depth (Pan et al., 2024). Therefore, it is imperative to conduct an in-depth investigation into the distribution characteristics and influencing factors of soil TN, IN, and MBN.

China's drylands exhibit substantial climatic variation across different geographic zones. Owing to ongoing climate change, the degree of aridity in drylands—including hyper-arid, arid, semi-arid, and dry-subhumid regions—is projected to increase globally, expanding the total extent of these ecosystems by an estimated 10.0% by the end of the century (Feng and Fu, 2013). Increased aridity has been shown to reduce soil N availability on a global scale, leading to declines in ON stocks in dryland ecosystems (Delgado-Baquerizo et al., 2013). Meanwhile, programs such as the Three-North Shelter Forest Program and the Grain for Green Project have significantly impacted soil moisture (Deng and Shangguan, 2016) and soil N content (Schmidt et al., 2011). N inputs driven by human impacts have already doubled the amount of naturally fixed N in terrestrial ecosystems (Zhang et al., 2014). Thus, we hypothesized that aridity and human impacts are likely the principal drivers of N fraction alterations. Human impacts are expected to have a positive influence, whereas aridity is expected to have a negative effect. These opposing forces may, to some extent, counterbalance each other. Using data from 2076 soil samples collected at 173 sampling sites in the drylands of northern China and complementary environmental data, this study aimed to: (1) quantify the stocks, spatial distributions, and main drivers of TN, IN, and MBN in the surface soils of the drylands in northern China; (2) evaluate the impacts of different LULC types on each of these N fractions; and (3) determine the extent to which human impacts influence the changes in these N fractions. Therefore, disentangling their individual and interactive effects is critical to advance our understanding of N cycling and to predict future changes in these vulnerable ecosystems.

2 Materials and methods

2.1 Study area

The drylands of northern China covered a total area of about 6.6×10^6 km^2, which accounts for

about 64.6% of the country's territorial area (Fig. 1). The mean annual precipitation in these drylands is 304.0 mm, lower than the mean annual potential evapotranspiration of 814.9 mm. Moreover, there is substantial interannual variability in precipitation, particularly in hyper-arid regions (with a coefficient of variation of 0.23 and precipitation below 25.0 mm) and arid regions (with a coefficient of variation of 0.11 and precipitation ranging between 25.0 and 250.0 mm) (Li et al., 2021). These drylands support a wide array of ecotypes, including barren ecosystems (e.g., Taklimakan Desert, Gurbantunggut Desert, Badain Jaran Desert, Tengger Desert, Kumtag Desert, Qaidam Basin, Hobq Desert, and Ulan Buh Desert), various grassland types (temperate meadow, temperate steppe, temperate barren steppe, alpine meadow, alpine steppe, and alpine barren steppe), glacial tundra (primarily on the Qinghai–Xizang Plateau), boreal forests (deciduous broad-leaved, evergreen coniferous, deciduous coniferous, and mixed coniferous-broad-leaved forests), and shrublands. Consequently, the structure and functioning of northern China's dryland ecosystems are complex and dynamic and characterized by numerous interconnected ecological processes (Li et al., 2021).

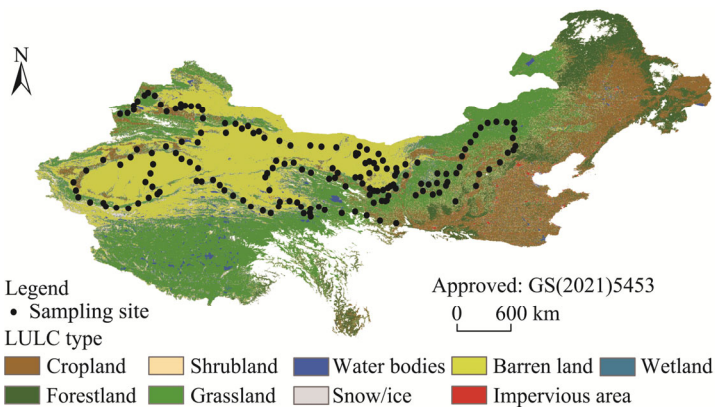

Fig. 1 Overview of the drylands in northern China based on the land use/land cover (LULC) data and distribution of sampling sites. Note that the figure is based on the standard map (GS(2021)5453) of the Map Service System (http://bzdt.ch.mnr.gov.cn/), and the standard map has not been modified.

2.2 Field sampling and experimental analysis

2.2.1 Field survey and sampling

To investigate the stocks of TN, IN, and MBN in the drylands of northern China and address associated scientific questions, we conducted extensive field surveys during the summers of 2021 and 2022, primarily along major transportation routes within the region. The selection of sampling sites followed the criteria outlined by Zhang et al. (2022): (1) ensuring an even distribution of sampling sites across the drylands of northern China; and (2) maintaining a minimum distance of 3 km from roads to minimize potential anthropogenic disturbances. In total, we surveyed 173 sampling sites, spanning longitudes from 77°19′48″E to 116°11′24″E and latitudes from 35°33′00″N to 46°21′36″N, thereby encompassing the climatic gradients and major LULC types representative of these drylands. At each sampling sites, we established a 10 m×10 m plot and collected soil samples from three sampling points arranged along the diagonal of each plot. Samples were collected separately from 4 depth layers: 0–5, 5–10, 10–20, and 20–30 cm, resulting in a total of 2076 soil samples.

2.2.2 Soil sample preparation and laboratory determination

The soil samples were air-dried in the laboratory for a period of two to three weeks. They were then passed through a 2.00 mm sieve to remove fine roots. The processed samples were ground via a ball mill and subsequently passed through a 0.15 mm sieve. For TN analysis, 1.8 g of soil was weighed and placed into a digestion tube (60 parallel samples were processed per batch). Subsequently, 4 mL of concentrated H_2SO_4 was added, followed by four gradient additions of HF

at 10-min intervals. Once the reaction stabilized, five drops of 70.0% $HClO_4$ were added, and the mixture was oscillated and allowed to stand at room temperature for 12 h for predigestion. A gradient heating digestion program was then applied: 65°C for 1 h, followed by 120°C for 30 min, and finally 230°C for 1 h. After cooling to room temperature, the supernatant was transferred to a 100 mL volumetric flask for dilution. The quantitative analysis of TN was conducted via a BRAN+LUEBBE AA3 continuous flow analyzer (Seal AA3 Bran+Luebbe, Norderstedt, Germany), which strictly followed instrument protocols and quality control standards. For IN analysis, 10.0 g of fresh soil (sieved to 2.00 mm) was extracted with 2.0 mol/L KCl solution containing a nitrification inhibitor at a soil-to-solution ratio of 1:5. The mixture was shaken, centrifuged, and filtered. Ammonium N was determined via the indophenol blue method at 660 nm, and nitrate N was determined via the copper-cadmium reduction-sulfonamide coupling method at 540 nm, both of which used the BRAN+LUEBBE AA3 continuous flow analyzer. The detection limits for ammonium and nitrate N were 0.05 and 0.02 mg/kg, respectively. The system included a built-in dialysis module (10 kDa membrane) and an EDTA complexing system to eliminate interferences from high salts (Cl^- and Ca^{2+}) and silicates. The method achieved recoveries between 85.0% and 115.0%, with a relative standard deviation less than 8.0%, making it suitable for accurate analysis of IN in high-pH (9.2) barren soils. MBN density data were obtained from Gao et al. (2022), where MBN was determined using the chloroform fumigation-extraction method (Brookes et al., 1985). For this method, 5.0 g of fresh soil was weighed, placed in a 100 mL beaker, and then fumigated under vacuum at 25°C for 24 h in a desiccator containing chloroform and NaOH. After incubation, N was extracted using 0.5 mol/L K_2SO_4 (soil-to-solution ratio of 1.0:2.5). The N concentrations in the soil extracts were measured with a multi-N/C 3000 analyzer. The difference between the fumigated and non-fumigated samples was multiplied by a conversion factor of 0.45 to calculate the MBN density (Jenkinson et al., 2004). Bulk density was measured using the ring knife method. The soil sand content was estimated using the hydrometer and pipette method described by Kettler et al. (2001). The soil pH was determined using the potentiometric method with a water-to-soil ratio of 2.5:1.0.

2.3 Calculation of the TN and IN densities

Based on the obtained N concentration (N_h; g/kg), bulk density (BD_h; g/cm^3), proportion (%) of coarse fragments (>2.00 mm; C_h), and soil thickness (T_h; cm) at the soil depth layer h (h=1, 2, 3, 4), the soil N fraction density (SND; g/m^2) was calculated using Equation 1 (Tian et al., 2006; Yang, 2007; Kou et al., 2019):

$$\mathrm{SND} = \sum T_h \mathrm{BD}_h N_h \times (1 - C_h) / 100 . \quad (1)$$

Equation 2 was used to calculate each soil N fraction stock (Liu et al., 2011):

$$\mathrm{STNS} = \sum_{i=1}^{n} (D_i \times A \times 10^{-12}) , \quad (2)$$

where STNS (Tg) represents the soil N fraction stock within the study area; n denotes the total number of grid cells in the raster; D_i (g/m^2) is the TN, IN, or MBN density for the i^{th} grid cell; and A (m^2) is the area of each grid square, set by the defined resolution. In this study, the STNS was calculated for the upper 0–30 cm soil layer. These calculations were conducted via the ArcMap 10.3 with the spatial analyst module. Ordinary kriging was employed for spatial interpolation to generate surfaces covering the drylands of northern China. These surfaces were then converted into raster layers with a resolution of 1 km×1 km, where each raster cell contained a specific density value (g/m^2) and area (m^2).

2.4 Environmental data

The mean annual temperature data were obtained from the MOD11A1 V6 Global Climate Grid dataset within the MODIS data archive (https://doi.org/10.5067/MODIS/MOD11A1.006). The MOD11A1 V6 product provides daily surface temperature and emissivity values on a 1 km grid (Rodell et al., 2004). The Normalized Difference Vegetation Index (NDVI) was computed from Landsat remote sensing image bands, with a spatial resolution of 30 m. The aridity level at each

site was determined as 1–AI (Delgado-Baquerizo et al., 2013). AI data were sourced from the Global Aridity Index and Potential Evapotranspiration Climate database (https://cgiarcsi.community/). The LULC data were obtained from the European Space Agency Climate Change Initiative (ESA CCI) (https://climate.esa.int/en/) database, with a spatial resolution of 300 m. Global human impact data during 2000–2018 were accessed at a spatial resolution of 1 km, sourced from "A global record of annual terrestrial Human Footprint dataset from 2000 to 2018" (https://doi.org/10.1038/s41597-022-01284-8). This dataset included eight variables—the built environment, population density, nighttime lighting, farmland, pastureland, roads, railways, and navigable waterways—capturing diverse aspects of human pressure. These data were used following the methodology of Venter et al. (2016) to generate annual dynamic data on the global terrestrial human footprint for the period 2000–2020.

2.5 Estimation of the TN, IN, and MBN stocks

To obtain spatially explicit estimates of soil TN, IN, and MBN stocks, this study employed machine learning models to upscale site-level soil N fraction density to the regional scale. Machine learning models are recognized for their robustness in predicting soil and ecological properties over large areas (Beer et al., 2010). Compared with traditional upscaling methods based on taxonomic units, machine learning approaches can more effectively reduce uncertainty in soil carbon and N stock estimations (Ding et al., 2016; Kou et al., 2019). Three widely used machine learning models were selected: the Random Forest (RF) model, the eXtreme Gradient Boosting (XGBoost) model, and the Support Vector Machine (SVM) model. The soil TN, IN, and MBN stocks at 0–30 cm depth in the drylands of northern China were estimated via the following steps (Fig. 2).

First, three models—RF, XGBoost, and SVM—were constructed and validated via TN, IN, and MBN density data along with corresponding predictor variables. The predictor variables included human impacts, mean annual temperature, mean annual precipitation, NDVI, pH, clay content, and sand content. A random hierarchical partitioning strategy was used to split the dataset into a training set and a test set at a 75.0%:25.0% ratio. The training set was used for model parameter optimization, whereas the test set served as an independent validation dataset for the final performance assessment. To further evaluate model generalizability, a 5-fold cross-validation technique was employed during training. The training set was uniformly divided into five mutually exclusive subsets. In each of the five iterations, four subsets (80.0% of the training set) were used for model training, and one subset (20.0%) was used for hyperparameter tuning. The predictive performance of the three machine learning models was assessed using a 'leave-one-out' cross-validation approach. Model validation results were presented via 1:1 line plots. Additionally, the mean absolute error (MAE), root mean square error (RMSE), and coefficient of determination (R^2) were used to assess the models' strengths and weaknesses comprehensively. The optimal model was selected on the basis of the assessment accuracy to estimate the soil TN, IN, and MBN stocks in the study area. The formulas for MAE, RMSE, and R^2 are as follows:

$$\mathrm{MAE} = \frac{1}{m}\sum_{j=1}^{m}|P_j - O_j|, \tag{3}$$

$$\mathrm{RMSE} = \sqrt{\frac{1}{m}\sum_{j=1}^{m}(P_j - O_j)^2}, \tag{4}$$

$$R^2 = 1 - \frac{\sum_{j=1}^{m}(O_j - P_j)^2}{\sum_{j=1}^{m}(O_j - \bar{O})^2}, \tag{5}$$

where m represents the sample size; O_j and P_j represent the observed and predicted TN, IN, or MBN densities at site j, respectively; and $\bar{O}$ represents the mean of the observations. The closer

the MAE and RMSE are to zero, the greater the prediction accuracy; and the closer the R^2 is to 1.00, the greater the model fit. In this study, all the data were preprocessed—including mosaicking, fusion, and resampling—to ensure a uniform spatial resolution of 1 km×1 km for subsequent analyses.

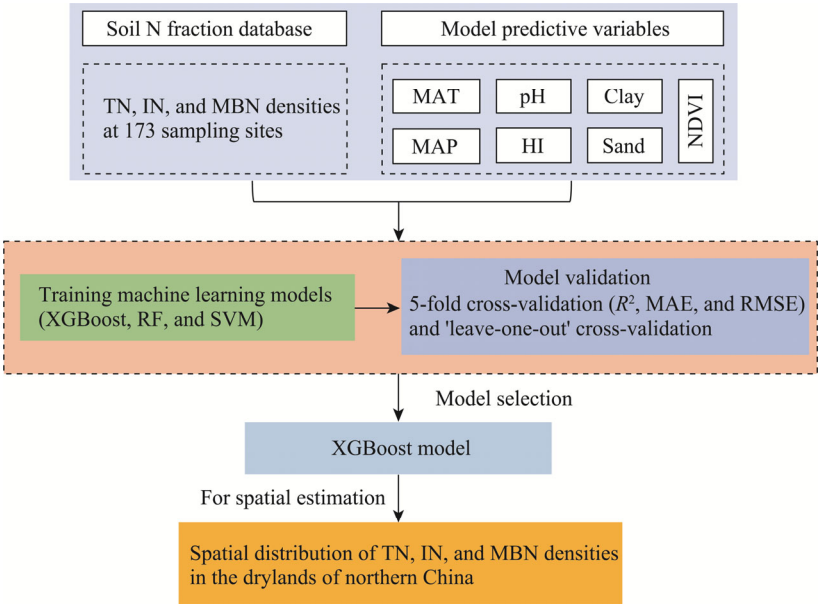

Fig. 2 Flow chart for estimating the TN, IN, and MBN stocks in this study. N, nitrogen; TN, total nitrogen; IN, inorganic nitrogen; MBN, microbial biomass nitrogen; MAT, mean annual temperature; MAP, mean annual precipitation; HI, human impacts; clay, soil clay content; sand, soil sand content; NDVI, Normalized Difference Vegetation Index; XGBoost, eXtreme Gradient Boosting; RF, Random Forest; SVM, Support Vector Machine; R^2, coefficient of determination; MAE, mean absolute error; RMSE, root mean square error.

2.6 Statistical analysis

To obtain spatially explicit estimates of soil N fraction stocks, we employed the best-performing XGBoost model to upscale soil N fraction densities from the site level to the regional scale. We used a Taylor diagram analysis at each sampling site to evaluate the performance of the XGBoost model in predicting the N fraction stocks. Spatial analyses were performed via ArcMap 10.3.

To examine the direct and indirect influences of environmental variables on soil N fraction changes, we applied the piecewise structural equation modeling (piecewiseSEM). Prior to modeling, the "selected forward" procedure was executed to identify the most significant predictors. In our piecewiseSEM framework, the climate and soil environmental factors were treated as composite variables. The model also accounted for random effects associated with different LULC types at the sampling sites. We calculated both marginal and conditional R^2 values: the marginal R^2 reflects the variance explained by fixed predictors alone, whereas the conditional R^2 accounts for variance explained by both fixed and random effects. Model fit was evaluated via Fisher's C test, with refinement on the basis of significance (P<0.050) and acceptable goodness-of-fit thresholds (0≤Fisher's C or df≤2 and 0.050<P≤1.000, where df is the degree of freedom). To determine the best predictors of N fraction variability, similar variables were included at different data scales within the piecewiseSEM. Standardized direct, indirect, and total effects were calculated for each predictor. The software packages used included "piecewiseSEM" (Lefcheck, 2016), "nlme", and "lme4". Additionally, the variance partitioning analysis (VPA) was performed using the "varpart" function in R 4.0.5 to quantify the relative contributions of climate factors, soil environmental factors, vegetation cover (indicated by NDVI), and human impacts to the variations in soil N fractions. The "MuMIn" package was used to analyze explanatory variables, whereas the "rdacca.hp" package was employed to assess their relative contributions (Gross et al., 2017).

3 Results

3.1 Evaluation of model prediction performance

The 1:1 line scatter plots illustrated the predictive performance of the three machine learning models for the TN, IN, and MBN densities in the drylands of northern China (Fig. 3). Among the three models, the XGBoost model presented the highest R^2 for all three N fractions, with R^2 values of 0.89 for MBN, 0.84 for IN, and 0.81 for TN. It also achieved the lowest MAE—0.7 g/m^2 for MBN, 3.8 g/m^2 for IN, and 76.9 g/m^2 for TN—and the lowest RMSE—1.0 g/m^2 for MBN, 5.6 g/m^2 for IN, and 106.9 g/m^2 for TN. These results suggested that the XGBoost model could effectively capture the spatial patterns of the soil TN, IN, and MBN stocks at large spatial scales.

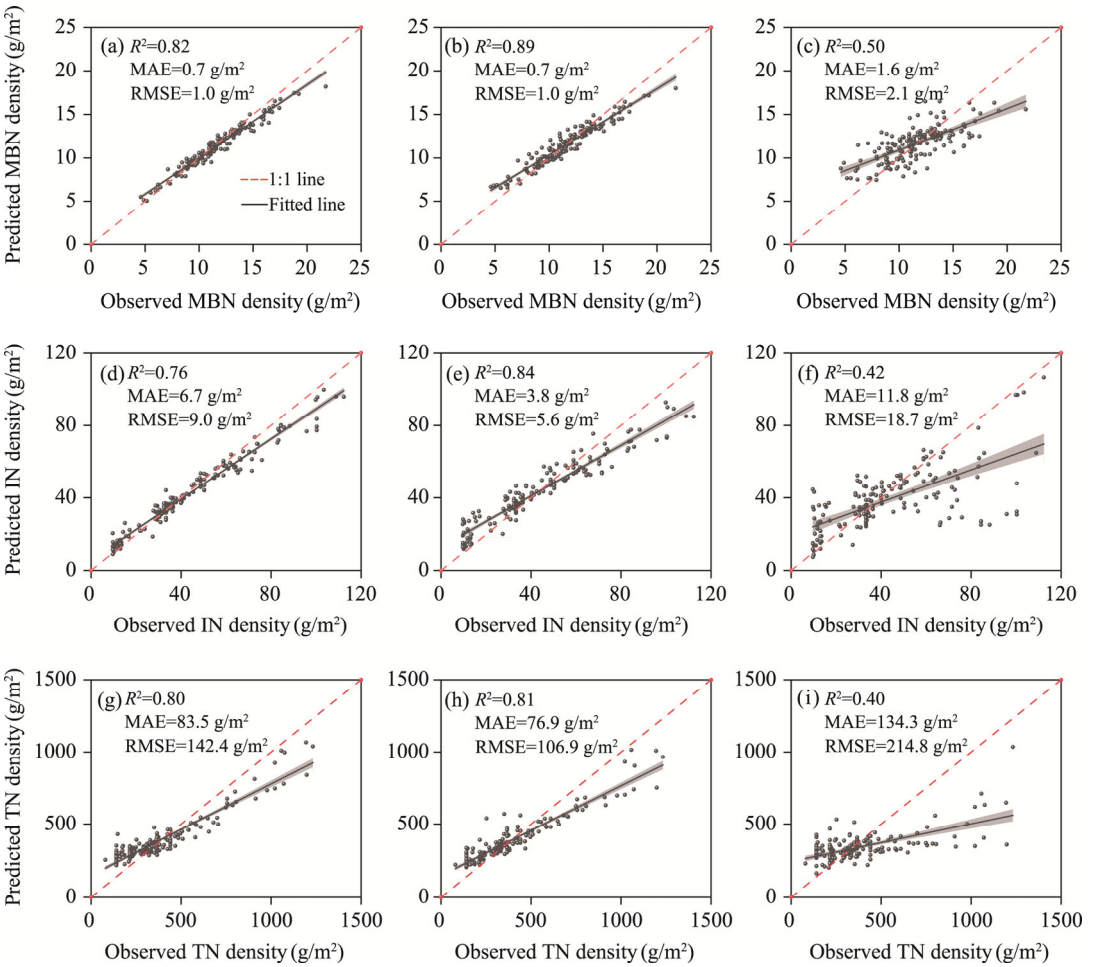

Fig. 3 Scatter plots indicating the effectiveness of the RF, XGBoost, and SVM models in predicting MBN (a–c), IN (d–f), and TN (g–i) densities in the drylands of northern China. The gray shading area represents the 95% confidence interval.

3.2 Spatial distribution characteristics of soil N fractions in the drylands of northern China

Geospatial analysis revealed that the spatial distributions of the soil TN, IN, and MBN densities across the drylands of northern China are highly consistent, with evident regional heterogeneity (Fig. 4). Areas with high soil N stocks were primarily concentrated in the frigid zone of the Qinghai–Xizang Plateau and the temperate zone of the Northeast China Plain. In contrast, low soil N stock areas were found in the barren lands, including the Junggar Basin, Taklimakan Desert, and Kumtag Desert.

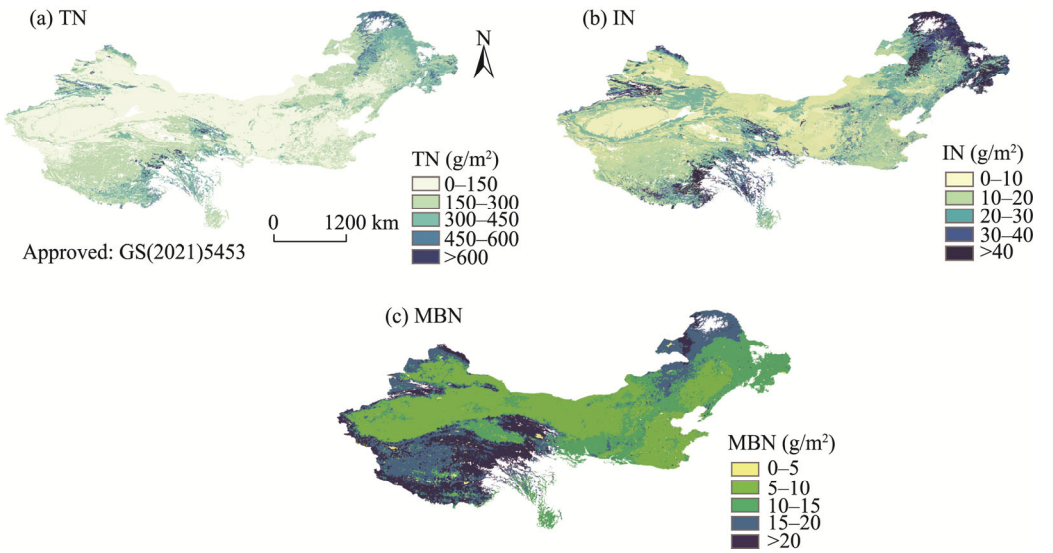

Fig. 4 Spatial distribution patterns of soil TN (a), IN (b), and MBN (c) densities in the drylands of northern China. Note that the figure is based on the standard map (GS(2021)5453) of the Map Service System (http://bzdt.ch.mnr.gov.cn/), and the standard map has not been modified.

At the 0–30 cm soil depth layer, the estimated stocks of TN, IN, and MBN in the study area were about 1020.4, 92.2, and 40.8 Tg, respectively. The corresponding mean densities were estimated at 164.6, 14.9, and 6.6 g/m^2, respectively (Table 1). Grassland soils presented the highest TN stock at about 420.4 Tg, accounting for about 41.2% of the total, whereas shrubland soils presented the lowest TN stock at about 53.8 Tg (5.3% of the total). The forestland soils presented the highest TN density (221.9 g/m^2), whereas the soils in barren land presented the lowest (70.1 g/m^2). For IN density, forestland soils again ranked the highest (20.5 g/m^2), whereas the soils in barren land were the lowest (9.5 g/m^2). In terms of MBN density, forestland soils presented the highest value (8.3 g/m^2), and the soils in barren land presented the lowest value (3.7 g/m^2).

Table 1 Estimation of densities and stocks of soil nitrogen (N) fractions for different land use/land cover (LULC) types in the drylands of northern China

LULC type	TN		IN		MBN	
	Density (g/m^2)	Stock (Tg)	Density (g/m^2)	Stock (Tg)	Density (g/m^2)	Stock (Tg)
Cropland	199.1	162.5	16.9	13.8	7.6	6.2
Forestland	221.9	170.7	20.5	15.7	8.3	6.4
Shrubland	200.5	53.8	16.3	4.4	6.1	1.6
Grassland	190.7	420.2	16.2	35.7	7.4	16.3
Barren land	70.1	122.1	9.5	16.6	3.7	6.5
Others	183.7	91.1	12.1	6.0	7.7	3.8
Mean	164.6	-	14.9	-	6.6	-
Total	-	1020.4	-	92.2	-	40.8

Note: TN, total nitrogen; IN, inorganic nitrogen; MBN, microbial biomass nitrogen.

3.3 Main drivers of soil N fraction changes in the drylands of northern China

This study further investigated the regulatory factors influencing changes in soil N fractions within the dryland ecosystems using the piecewiseSEM (Fig. 5). The combined influence of climate factors, soil environmental factors, NDVI, and human impacts significantly explained the variations in TN (marginal R^2=0.47), IN (marginal R^2=0.43), and MBN (marginal R^2=0.23). When accounting for the random effects of the 'sampling site', the model explained an increase of approximately 20.0% of the variation in soil N fractions.

The piecewiseSEM results indicated that mean annual precipitation, aridity, and human impacts not only have strong direct effects on soil N fractions but also contribute significantly through indirect pathways. The VPA further revealed that climate factors, soil environmental factors, NDVI, and human impacts collectively explained 37.5%–64.5% of the observed variation in N fractions (Fig. 6). Among these factors, climate factors exerted the most substantial independent influence, contributing between 6.9% and 33.7%. Human impacts and soil environmental factors also made notable independent contributions, ranging from 6.6% to 10.4% and 5.4% to 15.2%, respectively. NDVI had a relatively small independent effect, contributing between 0.0% and 1.8%. Notably, the interaction between climate and soil environmental factors exceeded the impact of their individual effects.

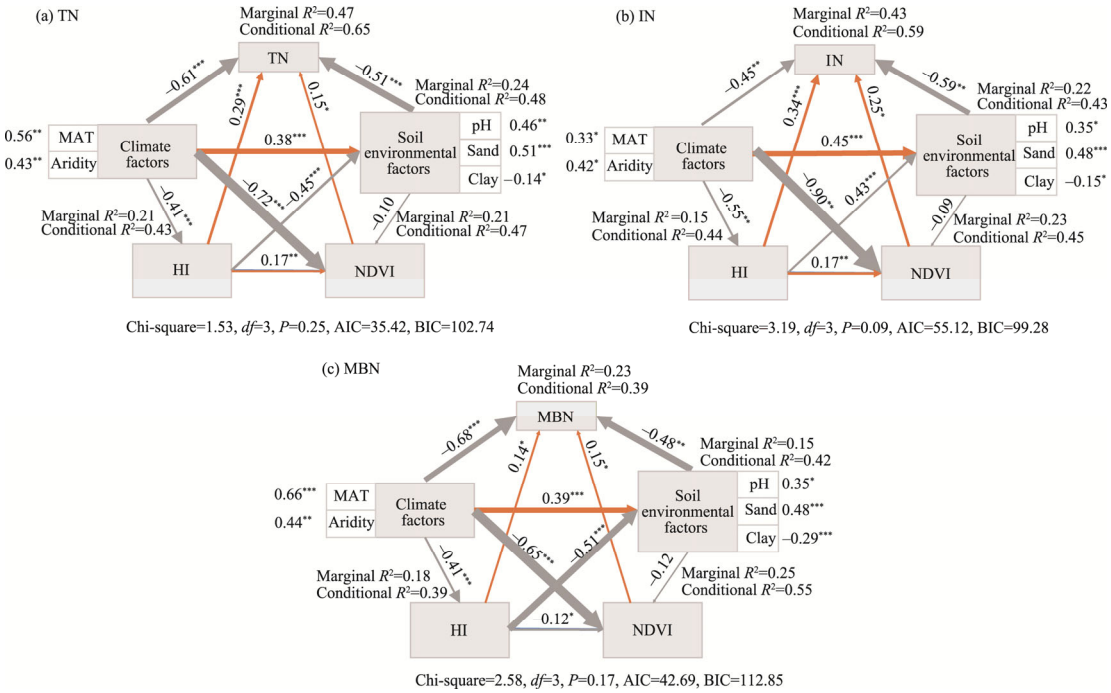

Fig. 5 Piecewise structural equation modeling (PiecewiseSEM) accounting for the direct and indirect effects of different predictors on TN (a), IN (b), and MBN (c) in the drylands of northern China. The gray arrows indicate negative correlations, and the orange arrows indicate positive correlations. The thickness of the arrow is proportional to the magnitude of standardized path coefficients and indicative of the strength of the relationship. The coefficients adjacent to the climate and soil environmental factors represent the independent effects of each factor. Marginal R^2 and conditional R^2 denote the proportion of variance explained by the included predictors without and with accounting for random effects of the 'sampling site', respectively. *df*, degree of freedom; AIC, Akaike Information Criterion; BIC, Bayesian Information Criterion. *, P<0.050 level; **, P<0.010 level; ***, P<0.001 level.

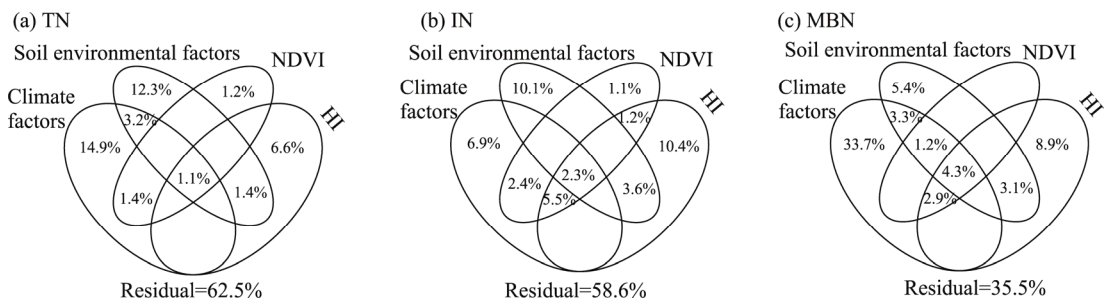

Fig. 6 Variance partitioning analysis (VPA) revealing the relative contributions of different environmental factors to the variations in TN (a), IN (b), and MBN (c) in the drylands of northern China. Only positive relative contributions are shown in the figure. Residual indicates the portion of variation in the target variable that cannot be explained by the model.

4 Discussion

4.1 Superiority of the XGBoost model

This study demonstrated that the XGBoost model performs exceptionally well in modeling soil N fractions in the drylands of northern China. This is primarily due to its capacity to capture complex nonlinear relationships, its efficient feature importance screening mechanism, and its resistance to overfitting (Chi et al., 2022). Compared with traditional statistical methods (e.g., multiple linear regression), the XGBoost model effectively captures higher-order interactions among multiple variables—such as soil pH, organic matter content, and microbial activity—by integrating a gradient boosting framework with multiple decision trees. Its built-in regularization terms (L1/L2) constrain model complexity, making it particularly well suited for environmental datasets characterized by high dimensionality and multicollinearity, such as soil spectral data. Therefore, the XGBoost model should be more widely adopted in future large-scale environmental studies.

4.2 Characteristics of each soil N fraction

Our study revealed that at the 0–30 cm of soil depth layer across the drylands of northern China, the TN stock is 1020.4 Tg, with an average N density of 164.6 g/m^2. In contrast, Yang et al. (2007) estimated the TN stock in China's surface soils (depth of 0–30 cm) at 3.39 Pg, with an average density of 0.4 kg/m^2, on the basis of 2473 soil profiles from the national soil census. These findings indicated that although drylands occupy about 64.6% of China's land area, the TN stock in dryland surface soils accounts for only 32.7% of the national total. This disparity can be attributed to several environmental factors. Lower precipitation and higher evapotranspiration in drylands reduce salt leaching, resulting in the accumulation of calcium carbonate and gypsum, high base saturation, and characteristically high soil pH (Ewing et al., 2006). Compared with humid regions, soils in drylands have coarser textures and lower organic matter contents, which lead to reduced water retention, increased bulk density, and lower cation exchange capacity (Ren et al., 2024). These conditions contribute to reduced soil N levels. Furthermore, drylands receive fewer organic matter inputs from leaf litter and root systems, which are more abundant in humid environments (Paul et al., 2002). This results in decreased nutrient input to the soil (Li et al., 2012), contributing to the lower TN stocks observed in dryland regions. The decline in N content with increasing aridity is driven primarily by reduced soil water availability and vegetation cover—both of which directly or indirectly influence N-related processes, particularly biological functions such as photosynthesis, atmospheric N fixation, and the activity of soil microbes and enzymes (Li et al., 2007; Reynolds et al., 2007; Vicente-Serrano et al., 2012). Rising temperatures associated with arid conditions may intensify the effects of drought on N availability. Additionally, reduced vegetation cover and elevated temperatures can lead to increased soil drying and erosion, promoting the loss of fine, nutrient-rich particles such as clay (Reynolds et al., 2007). These processes contribute to a reduction in soil N under arid conditions.

4.3 Impact of LULC on variations in soil N fractions

This study highlighted significant variations in the density of soil N fractions across different LULC types. Previous research has consistently demonstrated that differences in vegetation cover and soil management practices under various LULC types lead to substantial variability in N density (Wang et al., 2012; Gao et al., 2020; Uwiragiye et al., 2024), which aligns with our findings. Human-induced changes in LULC exert considerable impacts on soil nutrients, as evidenced in this study by the highest density of N fractions observed in forestlands and the lowest density in barren land.

Changes in LULC result in shifts in plant species composition, abundance, and chemical characteristics, which in turn play pivotal roles in N sequestration (Gao et al., 2020). Notably, dynamic changes in N fractions arise from land use practices and management strategies, especially under significant LULC transformations (Gross and Harrison, 2019). Soil N stocks

tend to increase when land is converted from cropland to forestland and/or grassland (Deng and Shangguan, 2016; Liang et al., 2023). Meena et al. (2018) emphasized that restoring degraded cropland to grassland and woodland can increase N stocks in India's Central Himalayan region. These findings consistently support the conclusion in this study that soil N stocks in forestland or grassland exceeded those in cropland.

Soil pH and moisture content, which are key factors affected by LULC changes, significantly influence the rates of N mineralization and nitrification (Knoepp and Swank, 2002; Mikan et al., 2002). Compared with forestland and grassland, soils in barren land typically present a lower moisture content and higher alkalinity. These conditions lead to reduced soil microbial activity (Zhang et al., 2022) and lower mineralization and nitrification rates (Knoepp and Swank, 2002; Zheng et al., 2020), ultimately resulting in lower IN and MBN densities. Additionally, Deng et al. (2021) demonstrated that aridity decreases the rates of N mineralization by 5.7% and nitrification by 13.8%, thereby reducing the soil IN density. Aridity also contributes to reduced MBN density by suppressing microbial activity (Zhu et al., 2021) and lowering the abundance of soil bacteria and fungi (Xi et al., 2022).

4.4 Impacts of human impacts on soil N fractions

Our study revealed that human impacts have a significantly positive effect on soil TN. This increase in soil N due to human activities can be attributed to four primary factors. First, anthropogenic fertilization leads to an increase in the soil N content. Dang et al. (2022) reported a notable increase in soil TN under long-term fertilizer and straw return treatment. The application of organic fertilizers or straw improves soil structure, enhances aggregation, reduces N loss, increases the proportion of larger aggregates, and indirectly elevates soil N fraction stocks (Sodhi et al., 2009; He et al., 2015; Iqbal et al., 2018). Second, grazing activities significantly affect soil N levels (Zhou et al., 2017; Chen et al., 2023). Intensive grazing increases soil TN through the deposition of manure and urine by livestock, with the effect intensifying as the number of grazing events increases—particularly in the later stages of rotation. The increase in soil N is largely due to the addition of readily available N from animal waste. Grazing animals return most of the consumed plant nutrients back to the soil (Haynes and Williams, 1993; Sun et al., 2018). Third, human impacts contribute to elevated atmospheric nitrogenous compounds, leading to N deposition. Ochoa-Hueso et al. (2014) reported that N deposition in semi-arid mesocosm ecosystems increases both soil carbon and N levels. China, identified as a hotspot for N deposition, may continue to experience prolonged elevated deposition levels (Jia et al., 2014), thereby contributing to increased soil N content. Finally, dynamic changes in the TN stock may result from significant alterations in land use and management (Rumpel and Kögel-Knabner, 2010; Gross and Harrison, 2019). Current national initiatives—such as the Grain for Green Project and the Three-North Shelter Forest Program—have significantly impacted soil N levels (Schmidt et al., 2011). In arid and semi-arid areas, afforestation, especially with broad-leaved deciduous species, has been shown to increase soil organic carbon accumulation by 131.0% and TN accumulation by 88.0% (Liu et al., 2018).

4.5 Impacts of aridity on soil N fractions

Our findings indicated that aridity and human impacts are the dominant drivers of TN density variation in the drylands of northern China, exerting opposing influences. It is a consistent conclusion that aridity reduces soil TN. For example, Delgado-Baquerizo et al. (2013) reported that TN decreases in dryland regions, likely due to increased soil erosion and reduced vegetation cover under increasing aridity. In nutrient-limited ecosystems (Schlesinger et al., 1990), the suppression of N mineralization may trigger a positive feedback loop that further limits nutrient availability (Schimel and Bennett, 2004). Intensified water scarcity further suppresses microbial activity in drylands by limiting nutrient availability (Maestre et al., 2015). Under desiccation, soil microbes survive as dormant inocula by accumulating solutes within cells—requiring both carbon and N to lower the water potential and maintain hydration (Schimel et al., 2007). This response

slows N cycling and leads to reduced TN in the soil. Dryland ecosystems are also characterized by high-intensity but infrequent rainfall events (Dijkstra et al., 2012), which induce a stronger response in soil microbial communities than in plant growth (Collins et al., 2008). Since microbial mineralization of organic matter is a major source of soil IN (Sirulnik et al., 2007), rainfall-driven microbial activation may lead to substantial N release. However, when moisture availability limits plant N uptake, desynchronization in the N cycle occurs, resulting in N losses via nitrification and denitrification (Knapp et al., 2008). Consequently, the increase in gaseous N losses with increasing aridity outweighs the primary mechanism contributing to net plant N accumulation. Ammonia volatilization—characterized by a high isotope fractionation factor (Handley et al., 1999)—represents a significant abiotic pathway for N loss, particularly in extremely arid regions where elevated soil pH level, a key factor driving ammonia volatilization, is commonly observed (Wang et al., 2014). Thus, as aridity increases, both N_2O and ammonia emissions from the soil intensify, resulting in further depletion of soil N fraction stocks.

The impacts of aridity and human impacts on N dynamics can offset each other. Delgado-Baquerizo et al. (2016) reported that, globally, N limitation tends to intensify in most arid regions. However, in hyper-arid zones, the increase in N resulting from human impacts may counterbalance the potential increase in N limitation. This phenomenon may be attributed to the constraints imposed by aridity—such as reduced water availability—that can limit both human impacts and overall urban development (Li et al., 2021). The significant negative correlation between human impacts and aridity proxies reveals a key spatial disparity: aridity promotes N loss, while human activities lead to N accumulation across dryland regions (Liu et al., 2010). For example, overgrazing in grassland ecosystems can cause soil degradation, soil erosion, and considerable losses of nutrients, including N and phosphorus (Niu et al., 2015). Aridity has been shown to increase the mineral N content by 31.0% but decrease the N mineralization and nitrification rates by 5.7% and 13.8%, respectively, resulting in relatively stable TN contents (Deng et al., 2021). This study also demonstrated that temperature is a critical driver of spatial variation in N, with a significant negative effect on both TN and its associated fractions. Delgado-Baquerizo et al. (2016) further highlighted that the strong negative correlation between human impacts and aridity suggests a current spatial disconnect between aridity-driven N losses and human impact-driven N accumulation in different dryland ecosystems (Liu et al., 2010). Thus, on a global scale, while N limitation is expected to intensify in the hyper-arid areas, the increase in N inputs through human impacts in less arid drylands may offset any overall trend toward increased N limitation.

4.6 Limitations and uncertainties

In this study, the sampling sites are distributed mainly in natural areas, and there is a lack of data in artificial restoration areas and oasis areas in arid regions, which may lead to an underestimation of the situation in the corresponding areas. Previous studies have shown that only IN—a small fraction (2.0%–8.0%) of TN—is readily available for plant uptake. In this study, the estimated ratio of IN to TN was 0.09, which may reflect an underestimation of TN stock or an overestimation of IN stock in dryland areas. Biological soil crusts, which are widely present in arid and semi-arid areas, play vital roles in soil ecology, hydrology, and nutrient cycling, contributing significantly to N and carbon inputs via N fixation and photosynthesis. However, the exclusion of soils under biological crusts from the sampling strategy may have led to an underestimation of TN stock and a corresponding inflation in the relative share of IN. The MBN data utilized in this study were derived from Gao et al. (2022) and were not obtained through direct soil sample analysis. This reliance introduces potential uncertainties in the estimation of MBN stock. Vegetation may have an important influence on variations in soil N fractions in dryland areas. However, our study revealed that the contribution of vegetation to variations in N fractions is small. The use of NDVI to characterize the effects of vegetation has several limitations. NDVI can characterize only the above-ground portion of vegetation, while the sampling sites in this study was concentrated in barren areas where the differences in NDVI were

not significant. Since vegetation in barren land has a well-developed root system, this study ignored the moderating effect of the plant root system on the N fractions. In addition, due to the relatively coarse spatial scale, this study may not have fully captured the plant patch effects, as they are likely obscured by data homogenization. Additionally, the air-dried samples substantially increased the ratios of IN to TN in this study.

5 Conclusions

Our study compared the predictive performance of three machine learning models on the basis of 2076 soil samples collected from 173 sites in the drylands of northern China. The XGBoost model, which performed the best, was selected to estimate and spatially map the soil N fraction stocks. Although the densities of TN, IN, and MBN in drylands were significantly lower than those in other regions of China, the considerable area proportion of drylands resulted in considerably higher reserves of the N fractions in these regions. LULC changes had notable effects on soil N dynamics. The VPA and piecewiseSEM found that climate factors and human impacts jointly dominate the changes in N fractions and that the two kinds of factors have mutually offsetting antagonistic effects. Our findings are crucial for reducing uncertainty in N fraction estimations at national and global scales and offer valuable insights for developing targeted soil N management strategies in drylands. For example, afforestation in arid wastelands can markedly increase soil N fraction stocks. Similarly, N inputs in arid croplands should be adjusted according to local aridity levels, while pasture growth and grazing intensity should be key indicators for managing grasslands under different aridity regimes.

Conflict of interest

ZHOU Xiaobing and ZHANG Yuanming are editorial board members of Journal of Arid Land and were not involved in the editorial review or the decision to publish this article. All authors declare that there are no competing interests.

Acknowledgements

This work was supported by the Xinjiang Outstanding Youth Fund (2021D01E03), the Natural Science Foundation of Xinjiang Uygur Autonomous Region (2022D01D083), and the National Natural Science Foundation of China (U2003214, 41977099). Thanks to Dr. LU Yongxing and Dr. GUO Xing for their help in field sampling.

Author contributions

Conceptualization: ZHANG Shihang, ZHOU Xiaobing, ZHANG Yuanming; Data curation: CHEN Yusen; Writing - original draft preparation: ZHANG Shihang; Writing - review and editing: ZHANG Shihang, CHEN Yusen, ZHOU Xiaobing, ZHANG Yuanming; Funding acquisition: ZHOU Xiaobing, ZHANG Yuanming. All authors approved the manuscript.

References

Bardgett R D, van der Putten W H. 2014. Belowground biodiversity and ecosystem functioning. Nature, 515(7528): 505–511.

Beer C, Reichstein M, Tomelleri E, et al. 2010. Terrestrial gross carbon dioxide uptake: global distribution and covariation with climate. Science, 329(5993): 834–838.

Brookes P C, Landman A, Pruden G, et al. 1985. Chloroform fumigation and the release of soil nitrogen: A rapid direct extraction method to measure microbial biomass nitrogen in soil. Soil Biology & Biochemistry, 17(6): 837–842.

Chen S S, Wang M, Zhang C, et al. 2023. Impacts of grazing disturbance on soil nitrogen component contents and storages in a *Leymus chinensis* Meadow Steppe. Agronomy, 13(6): 1574, doi: 10.3390/agronomy13061574.

Chi Y L, Fan M, Zhao C F, et al. 2022. Machine learning-based estimation of ground-level NO_2 concentrations over China. Science of the Total Environment, 807(1): 150721, doi: 10.1016/j.scitotenv.2021.150721.

Collins S L, Sinsabaugh R L, Crenshaw C, et al. 2008. Pulse dynamics and microbial processes in aridland ecosystems. Journal

of Ecology, 96(3): 413–420.

Compton J E, Harrison J A, Dennis R L, et al. 2011. Ecosystem services altered by human changes in the nitrogen cycle: a new perspective for US decision making. Ecology Letters, 14(8): 804–815.

Cornell S E. 2011. Atmospheric nitrogen deposition: Revisiting the question of the importance of the organic component. Environmental Pollution, 159(10): 2214–2222.

Cui S H, Shi Y L, Groffman P M, et al. 2013. Centennial-scale analysis of the creation and fate of reactive nitrogen in China (1910–2010). Proceedings of the National Academy of Sciences of the United States of America, 110(6): 2052–2057.

Dang P F, Li C F, Huang T T, et al. 2022. Effects of different continuous fertilizer managements on soil total nitrogen stocks in China: A meta-analysis. Pedosphere, 32(1): 39–48.

Davidson E A, Janssens I A. 2006. Temperature sensitivity of soil carbon decomposition and feedbacks to climate change. Nature, 440(7081): 165–173.

Delgado-Baquerizo M, Maestre F T, Gallardo A, et al. 2013. Decoupling of soil nutrient cycles as a function of aridity in global drylands. Nature, 502(7473): 672–676.

Delgado-Baquerizo M, Maestre F T, Gallardo A, et al. 2016. Human impacts and aridity differentially alter soil N availability in drylands worldwide. Global Ecology and Biogeography, 25(1): 36–45.

Deng L, Shangguan Z P. 2016. Afforestation drives soil carbon and nitrogen changes in China. Land Degradation & Development, 28(1): 151–165.

Deng L, Peng C H, Kim D G, et al. 2021. Drought effects on soil carbon and nitrogen dynamics in global natural ecosystems. Earth-Science Reviews, 214: 103501, doi: 10.1016/j.earscirev.2020.103501.

Dentener F, Drevet J, Lamarque J F, et al. 2006. Nitrogen and sulfur deposition on regional and global scales: A multimodel evaluation. Global Biogeochemical Cycles, 20(4): GB4003, doi: 10.1029/2005GB002672.

Dijkstra F A, Augustine D J, Brewer P, et al. 2012. Nitrogen cycling and water pulses in semiarid grasslands: are microbial and plant processes temporally asynchronous? Oecologia, 170(3): 799–808.

Ding J Z, Li F, Yang G B, et al. 2016. The permafrost carbon inventory on the Tibetan Plateau: a new evaluation using deep sediment cores. Global Change Biology, 22(8): 2688–2701.

Durán J, Delgado-Baquerizo M, Dougill A J, et al. 2018. Temperature and aridity regulate spatial variability of soil multifunctionality in drylands across the globe. Ecology, 99(5): 1184–1193.

Elrys A S, Uwiragiye Y, Zhang Y H, et al. 2023. Expanding agroforestry can increase nitrate retention and mitigate the global impact of a leaky nitrogen cycle in croplands. Nature Food, 4(1): 109–121.

Elrys A S, El-Maati M F A, Dan X Q, et al. 2024. Aridity creates global thresholds in soil nitrogen retention and availability. Global Change Biology, 30(1): e17003, doi: 10.1111/gcb.17003.

Ewing S A, Sutter B, Owen J, et al. 2006. A threshold in soil formation at Earth's arid-hyperarid transition. Geochimica et Cosmochimica Acta, 70(21): 5293–5322.

Feng S, Fu Q. 2013. Expansion of global drylands under a warming climate. Atmospheric Chemistry and Physics, 13(19): 10081–10094.

Fujimaki R, Sakai A, Kaneko N. 2009. Ecological risks in anthropogenic disturbance of nitrogen cycles in natural terrestrial ecosystems. Ecological Research, 24(5): 955–964.

Galloway J N, Dentener F J, Capone D G, et al. 2004. Nitrogen cycles: past, present, and future. Biogeochemistry, 70(2): 153–226.

Gao D C, Bai E, Wang S Y, et al. 2022. Three-dimensional mapping of carbon, nitrogen, and phosphorus in soil microbial biomass and their stoichiometry at the global scale. Global Change Biology, 28(22): 6728–6740.

Gao G Y, Tuo D F, Han X Y, et al. 2020. Effects of land-use patterns on soil carbon and nitrogen variations along revegetated hillslopes in the Chinese Loess Plateau. Science of the Total Environment, 746: 141156, doi: 10.1016/j.scitotenv.2020.141156.

Gross C D, Harrison R B. 2019. The case for digging deeper: soil organic carbon storage, dynamics, and controls in our changing world. Soil Systems, 3(2): 28, doi: 10.3390/soilsystems3020028.

Gross N, Bagousse-Pinguet Y L, Liancourt P, et al. 2017. Functional trait diversity maximizes ecosystem multifunctionality. Nature Ecology & Evolution, 1(5): 132, doi: 10.1038/s41559-017-0132

Handa I T, Aerts R, Berendse F, et al. 2014. Consequences of biodiversity loss for litter decomposition across biomes. Nature, 509: 218–221.

Handley L L, Austin A T, Robinson D, et al. 1999. The ^{15}N natural abundance (δ15N) of ecosystem samples reflects measures of water availability. Australian Journal of Botany, 26: 185–199.

Haynes R J, Williams P H. 1993. Nutrient cycling and soil fertility in the grazed pasture ecosystem. Advances in Agronomy, 49:

119–199.
He N P, Yu Q, Wu L, et al. 2008. Carbon and nitrogen store and storage potential as affected by land-use in a *Leymus chinensis* grassland of northern China. Soil Biology & Biochemistry, 40(12): 2952–2959.
He Y T, Zhang W J, Xu M G, et al. 2015. Long-term combined chemical and manure fertilizations increase soil organic carbon and total nitrogen in aggregate fractions at three typical cropland soils in China. Science of the Total Environment, 532: 635–644.
Heuck C, Weig A, Spohn M. 2015. Soil microbial biomass C:N:P stoichiometry and microbial use of organic phosphorus. Soil Biology & Biochemistry, 85: 119–129.
Hu H W, Trivedi P, He J Z, et al. 2017. Microbial nitrous oxide emissions in dryland ecosystems: mechanisms, microbiome and mitigation. Environmental Microbiology, 19(12): 4808–4828.
Huang J P, Yu H P, Guan X D, et al. 2016. Accelerated dryland expansion under climate change. Nature Climate Change, 6(2): 166–171.
Iqbal S, Khan H Z, Li T, et al. 2018. Organic nitrogen source addition for improving the physicochemical properties of sandy loam soil and maize performance. Communications in Soil Science and Plant Analysis, 49(1): 13–29.
Jenkinson D S, Brookes P C, Powlson D S. 2004. Measuring soil microbial biomass. Soil Biology & Biochemistry, 36(1): 5–7.
Jia Y L, Yu G R, He N P, et al. 2014. Spatial and decadal variations in inorganic nitrogen wet deposition in China induced by human activity. Scientific Reports, 4: 3763, doi: 10.1038/srep03763.
Kettler T A, Doran J W, Gilbert T L. 2001. Simplified method for soil particle-size determination to accompany soil-quality analyses. Soil Science Society of America Journal, 65(3): 849–852.
Knapp A K, Beier C, Briske D D, et al. 2008. Consequences of more extreme precipitation regimes for terrestrial ecosystems. Bioscience, 58(9): 811–821.
Knoepp J D, Swank W T. 2002. Using soil temperature and moisture to predict forest soil nitrogen mineralization. Biology and Fertility of Soils, 36(3): 177–182.
Kou D, Ding J Z, Li F, et al. 2019. Spatially-explicit estimate of soil nitrogen stock and its implication for land model across Tibetan alpine permafrost region. Science of the Total Environment, 650(2): 1795–1804.
Lefcheck J S. 2016. PiecewiseSEM: piecewise structural equation modeling in R for ecology, evolution, and systematics. Methods in Ecology and Evolution, 7(5): 573–579.
Li C J, Fu B J, Wang S, et al. 2021. Drivers and impacts of changes in China's drylands. Nature Reviews Earth & Environment, 2(12): 858–873.
Li D J, Niu S L, Luo Y Q. 2012. Global patterns of the dynamics of soil carbon and nitrogen stocks following afforestation: a meta-analysis. New Phytologist, 195(1): 172–181.
Li J R, Okin G S, Alvarez L, et al. 2007. Quantitative effects of vegetation cover on wind erosion and soil nutrient loss in a desert grassland of southern New Mexico, USA. Biogeochemistry, 85(3): 317–332.
Liang C, VandenBygaart A J, MacDonald D, et al. 2023. Change in soil organic carbon storage as influenced by forestland and grassland conversion to cropland in Canada. Geoderma Regional, 33: e00648, doi: 10.1016/j.geodrs.2023e00648.
Liu J, You L Z, Amini M, et al. 2010. A high-resolution assessment on global nitrogen flows in cropland. Proceedings of the National Academy of Sciences of the United States of America, 107(17): 8035–8040.
Liu L, He X Y, Du H, et al. 2017a. The relationships among nitrogen-fixing microbial communities, plant communities, and soil properties in karst regions. Acta Ecologica Sinica, 37(12): 4037–4044. (in Chinese).
Liu X, Yang T, Wang Q, et al. 2018. Dynamics of soil carbon and nitrogen stocks after afforestation in arid and semi-arid regions: A meta-analysis. Science of the Total Environment, 618: 1658–1664.
Liu Y, Wang C H, He N P, et al. 2017b. A global synthesis of the rate and temperature sensitivity of soil nitrogen mineralization: Latitudinal patterns and mechanisms. Global Change Biology, 23(1): 455–464.
Liu Z P, Shao M A, Wang Y Q. 2011. Effect of environmental factors on regional soil organic carbon stocks across the Loess Plateau region, China. Agriculture, Ecosystems & Environment, 142(3–4): 184–194.
Liu Z P, Shao M A, Wang Y Q. 2013. Spatial patterns of soil total nitrogen and soil total phosphorus across the entire Loess Plateau region of China. Geoderma, 197–198: 67–78.
Luo Y Q, Su B, Currie W S, et al. 2004. Progressive nitrogen limitation of ecosystem responses to rising atmospheric carbon dioxide. Bioscience, 54(8): 731–739.
Maestre F T, Delgado-Baquerizo M, Jeffries T C, et al. 2015. Increasing aridity reduces soil microbial diversity and abundance in global drylands. Proceedings of the National Academy of Sciences of the United States of Americ, 112(51): 15684–15689.
Meena V S, Mondal T, Pandey B M, et al. 2018. Land use changes: Strategies to improve soil carbon and nitrogen storage pattern in the mid-Himalaya ecosystem, India. Geoderma, 321: 69–78.

Mikan C J, Schimel J P, Doyle A P. 2002. Temperature controls of microbial respiration in arctic tundra soils above and below freezing. Soil Biology & Biochemistry, 34(11): 1785–1795.

Niu X Y, Wang Y H, Yang H, et al. 2015. Effect of land use on soil erosion and nutrients in Dianchi Lake watershed, China. Pedosphere, 25(1): 103–111.

Ochoa-Hueso R, Arroniz-Crespo M, Bowker M A, et al. 2014. Biogeochemical indicators of elevated nitrogen deposition in semiarid Mediterranean ecosystems. Environmental Monitoring and Assessment, 186(9): 5831–5842.

Pan S Y, Song Y C, Yuan R Y, et al. 2024. Variations in soil inorganic nitrogen content under canopies of two shrubs in the Junggar Desert. Acta Prataculturae Sinica, 33(5): 183–195. (in Chinese)

Paul K I, Polglase P J, Nyakuengama J G, et al. 2002. Change in soil carbon following afforestation. Forest Ecology and Management, 168(1–3): 241–257.

Pinder R W, Bettez N D, Bonan G B, et al. 2013. Impacts of human alteration of the nitrogen cycle in the US on radiative forcing. Biogeochemistry, 114(1–3): 25–40.

Plaza C, Zaccone C, Sawicka K, et al. 2018. Soil resources and element stocks in drylands to face global issues. Scientific Reports, 8: 13788, doi: 10.1038/s41598-018-32229-0.

Powlson D S, Prookes P C, Christensen B T. 1987. Measurement of soil microbial biomass provides an early indication of changes in total soil organic matter due to straw incorporation. Soil Biology & Biochemistry, 19(2): 159–164.

Pu C, Kan Z R, Liu P, et al. 2019. Residue management induced changes in soil organic carbon and total nitrogen under different tillage practices in the North China Plain. Journal of Integrative Agriculture, 18(6): 1337–1347.

Ren Z B, Li C J, Fu B J, et al. 2024. Effects of aridification on soil total carbon pools in China's drylands. Global Change Biology, 30(1): e17091, doi: 10.1111/gcb.17091.

Reynolds J F, Stafford Smith D M, Lambin E F, et al. 2007. Global desertification: Building a science for dryland development. Science, 316(5826): 847–851.

Rillig M C, Mummey D L. 2006. Mycorrhizas and soil structure. New Phytologist, 171(1): 41–53.

Rodell M, Houser P R, Jambor U, et al. 2004. The global land data assimilation system. Bulletin of the American Meteorological Society, 85(3): 381–394.

Rumpel C, Kögel-Knabner I. 2010. Deep soil organic matter—a key but poorly understood component of terrestrial C cycle. Plant and Soil, 338(1–2): 143–158.

Sardans J, Peñuelas J, Estiarte M. 2008. Changes in soil enzymes related to C and N cycle and in soil C and N content under prolonged warming and drought in a Mediterranean shrubland. Applied Soil Ecology, 39(2): 223–235.

Schimel D S. 2010. Drylands in the Earth system. Science, 327(5964): 418–419.

Schimel J, Balser T C, Wallenstein M. 2007. Microbial stress-response physiology and its implications for ecosystem function. Ecology, 88(6): 1386–1394.

Schimel J P, Bennett J. 2004. Nitrogen mineralization: Challenges of a changing paradigm. Ecology, 85(3): 591–602.

Schlesinger W H, Reynolds J F, Cunningham G L, et al. 1990. Biological feedbacks in global desertification. Science, 247(4946): 1043–1048.

Schmidt B H M, Kalbitz K, Braun S, et al. 2011. Microbial immobilization and mineralization of dissolved organic nitrogen from forest floors. Soil Biology & Biochemistry, 43(8): 1742–1745.

Sirulnik A G, Allen E B, Meixner T, et al. 2007. Impacts of anthropogenic N additions on nitrogen mineralization from plant litter in exotic annual grasslands. Soil Biology & Biochemistry, 39(1): 24–32.

Sodhi G P S, Beri V, Benbi D K. 2009. Soil aggregation and distribution of carbon and nitrogen in different fractions under long-term application of compost in rice-wheat system. Soil and Tillage Research, 103(2): 412–418.

Spohn M. 2016. Element cycling as driven by stoichiometric homeostasis of soil microorganisms. Basic and Applied Ecology, 17(6): 471–478.

Sun J, Ma B B, Lu X Y. 2018. Grazing enhances soil nutrient effects: Trade-offs between aboveground and belowground biomass in alpine grasslands of the Tibetan Plateau. Land Degradation & Development, 29(2): 337–348.

Tian H Q, Wang S Q, Liu J Y, et al. 2006. Patterns of soil nitrogen storage in China. Global Biogeochemical Cycles, 20(1): GB1001, doi: 10.1016/j.scitotenv.2019.136201.

Uwiragiye Y, Wang J, Huang Y Y, et al. 2024. Global ecosystem nitrogen cycling reciprocates between land-use conversion and its reversal. Global Change Biology, 30(10): e17537, doi: 10.1111/gcb.17537.

Venter O, Sanderson E W, Magrach A, et al. 2016. Global terrestrial Human Footprint maps for 1993 and 2009. Scientific Data, 3: 160067, doi: 10.1038/sdata.2016.67.

Vicente-Serrano S M, Zouber A, Lasanta T, et al. 2012. Dryness is accelerating degradation of vulnerable shrublands in semiarid Mediterranean environments. Ecological Monographs, 82(4): 407–428.

Wang C, Wang X B, Liu D W, et al. 2014. Aridity threshold in controlling ecosystem nitrogen cycling in arid and semi-arid grasslands. Nature Communications, 5: 4799, doi: 10.1038/ncomms5799.

Wang S F, Wang X K, Ouyang Z Y. 2012. Effects of land use, climate, topography and soil properties on regional soil organic carbon and total nitrogen in the Upstream Watershed of Miyun Reservoir, North China. Journal of Environmental Sciences, 24(3): 387–395.

Wang X, Cui L L, Yang S H, et al. 2019. Human-induced changes in Holocene nitrogen cycling in North China: An isotopic perspective from sedimentary pyrogenic material. Geophysical Research Letters, 46(9): 4599–4608.

Xi N X, Chen D X, Bahn M, et al. 2022. Drought soil legacy alters drivers of plant diversity-productivity relationships in oldfield systems. Science Advances, 8(18): eabn3368, doi: 10.1126/sciadvabn3368.

Xu L, He N P, Yu G R. 2020. Nitrogen storage in China's terrestrial ecosystems. Science of the Total Environment, 709: 136201, doi: 10.1016/j.scitotenv.2019.136201.

Yang W, Zhang D, Cai X W, et al. 2023. Natural revegetation over ~ 160 years alters carbon and nitrogen sequestration and stabilization in soil organic matter on the Loess Plateau of China. CATENA, 220: 106647, doi: 10.1016/j.catena.2022.106647.

Yang Y H, Ma W H, Mohammat A, et al. 2007. Storage, patterns and controls of soil nitrogen in China. Pedosphere, 17(6): 776–785.

Zhan T. 2022. Effects and mechanism of nitrogen and phosphorus reduction combined with selenium on growth of Guanxi pomelo and soil nitrogen utilization. PhD Dissertation. Wuhan: Huazhong Agricultural University. (in Chinese)

Zhang C, Liu G B, Xue S, et al. 2013. Soil organic carbon and total nitrogen storage as affected by land use in a small watershed of the Loess Plateau, China. European Journal of Soil Biology, 54: 16–24.

Zhang K R, Cheng X L, Dang H S, et al. 2020. Biomass:N:K:Ca:Mg:P ratios in forest stands world-wide: Biogeographical variations and environmental controls. Global Ecology and Biogeography, 29(12): 2176–2189.

Zhang M Y, Wang K L, Liu H Y, et al. 2015. How ecological restoration alters ecosystem services: an analysis of vegetation carbon sequestration in the karst area of northwest Guangxi, China. Environmental Earth Sciences, 74(6): 5307–5317.

Zhang S H, Tao Y, Chen Y S, et al. 2022. Spatial pattern of soil multifunctionality and its correlation with environmental and vegetation factors in the Junggar Desert, China. Biodiversity Science, 30(8): 140–150. (in Chinese)

Zhang W T, Li S Y, Du X Z, et al. 2014. Accounting methods, uncertainties and influential factors of net anthropogenic nitrogen input (NANI). Acta Ecologica Sinica, 34(24): 7454–7464. (in Chinese)

Zheng M H, Zhou Z H, Zhao P, et al. 2020. Effects of human disturbance activities and environmental change factors on terrestrial nitrogen fixation. Global Change Biology, 26(11): 6203–6217.

Zhou G Y, Zhou X H, He Y H, et al. 2017. Grazing intensity significantly affects belowground carbon and nitrogen cycling in grassland ecosystems: A meta-analysis. Global Change Biology, 23(3): 1167–1179.

Zhu E X, Cao Z J, Jia J, et al. 2021. Inactive and inefficient: Warming and drought effect on microbial carbon processing in alpine grassland at depth. Global Change Biology, 27(10): 2241–2253.

Zhu J X, Wang Q F, He N P, et al. 2016. Imbalanced atmospheric nitrogen and phosphorus depositions in China: Implications for nutrient limitation. Journal of Geophysical Research: Biogeosciences, 121(6): 1605–1616.

Zhu Q L, Elrys A S, Liu L J, et al. 2025. Converting acidic forests to managed plantations reduces soil nitrogen loss by inhibiting autotrophic nitrification while inducing nitrate immobilization in the tropics. Biology and Fertility of Soils, 61(3): 595–607.